

From Bright Windows to Dark Spots: The Evolution of Melt Pond Optical Properties during Refreezing

Philipp Anhaus^{1,1}, Christian Katlein^{1,1}, Marcel Nicolaus^{2,2}, Mario Hoppmann^{3,3}, and Christian Haas^{4,4}

¹Alfred-Wegener-Institut Helmholtz-Zentrum für Polar- und Meeresforschung

²Alfred Wegener Institute

³AWI, Germany

⁴AWI

November 30, 2022

Abstract

Melt ponds have a strong impact on the Arctic surface energy balance and the ice-associated ecosystem because they transmit more solar radiation compared to bare ice. In the existing literature, melt ponds are considered as bright windows to the ocean, even during freeze-up in autumn. In the central Arctic during the summer-autumn transition in 2018, we encountered a situation where more snow accumulated on refrozen melt ponds compared to the adjacent bare ice, leading to a reduction in light transmittance of the ponds even below that of bare ice. Supporting results from a radiative transfer model suggest that melt ponds with a snow cover >0.04 m lead to lower light transmittance than adjacent bare ice. This scenario has not been described in the literature before, but has potentially strong implications for example on autumn ecosystem activity, oceanic heat budget and thermodynamic ice growth.

1 **From Bright Windows to Dark Spots: Snow Cover Controls Melt Pond Optical**
2 **Properties during Refreezing**

3
4 **P. Anhaus^{1*}, C. Katlein¹, M. Nicolaus¹, M. Hoppmann¹, C. Haas^{1,2}**

5
6 ¹Alfred-Wegener-Institut Helmholtz-Zentrum für Polar- und Meeresforschung, Bremerhaven,
7 Germany

8 ²Department of Environmental Physics, University of Bremen, Bremen, Germany

9
10 *Corresponding author: Philipp Anhaus (philipp.anhaus@awi.de)

11
12 **Key Points:**

- 13 • Refrozen melt ponds may collect a thicker snow cover compared to bare sea ice due to their
14 recessed topography
- 15 • Such snow-covered melt ponds transmit less light compared to bare ice of similar type
- 16 • This scenario has not been documented before and should be accounted for in studies
17 involving light in a refreezing Arctic Ocean

18

19 **Word count = 4232**

20

21 **Abstract**

22 Melt ponds have a strong impact on the Arctic surface energy balance and the ice-associated
23 ecosystem because they transmit more solar radiation compared to bare ice. In the existing
24 literature, melt ponds are considered as bright windows to the ocean, even during freeze-up in
25 autumn. In the central Arctic during the summer-autumn transition in 2018, we encountered a
26 situation where more snow accumulated on refrozen melt ponds compared to the adjacent bare ice,
27 leading to a reduction in light transmittance of the ponds even below that of bare ice. Supporting
28 results from a radiative transfer model suggest that melt ponds with a snow cover >0.04 m lead to
29 lower light transmittance than adjacent bare ice. This scenario has not been described in the
30 literature before, but has potentially strong implications for example on autumn ecosystem activity,
31 oceanic heat budget and thermodynamic ice growth.

32

33

34 **Plain Language Summary**

35 Arctic sea ice is covered with snow during autumn, winter and spring. During summer, melt ponds
36 evolve in response to surface melting. After snow fall starts again in autumn, these ponds can be
37 filled with a lot of snow compared to bare ice because of their recessed surface. Indeed, during an
38 expedition close to the North Pole in summer and autumn 2018, we measured a thick snow cover
39 on ponds. This thick snow cover reduced the light availability underneath the ponds to levels below
40 that underneath adjacent bare ice. This is a surprising finding, because it is different from the
41 established theory of high light availability underneath melt ponds during both summer and
42 autumn and how this is described in most computer models. It has consequences for our

43 understanding of the ice-associated ecosystem (organisms that live in and under sea ice). It might
44 also impact the mass and energy balance of central Arctic sea ice during summer-autumn transition
45 when new sea ice starts forming.

46

47 **1 Introduction**

48 Snow controls the optical properties and, thus, regulates the energy as well as the mass balance of
49 sea ice because of its high reflectivity (Grenfell and Maykut, 1977) and insulation (e.g., Sturm et
50 al., 1997). The snow cover of Arctic sea ice is highly variable in time and space (Webster et al.,
51 2018). The rougher the sea ice topography the more snow accumulates (Sturm et al., 2002; Massom
52 et al., 1997), for example at the lee sides of pressure ridges (Webster et al., 2018), at windward
53 sides of snow dunes (Dadic et al., 2013) and within the depression of melt ponds (Perovich et al.,
54 2003). In turn, the distribution of snow, especially snow dunes, influence melt pond formation
55 (Petrich et al., 2012a; Polashenski et al., 2012). Melt ponds also play a key role for the surface
56 energy budget (Nicolaus et al., 2012) and the mass balance of sea ice (Flocco et al., 2015), as well
57 as for the ice- and ocean-associated ecosystem (Arrigo, 2014). In general, in August-September
58 the melt pond coverage peaks (Perovich et al., 2002) and open and mature ponds evolve towards
59 refrozen and snow-covered ponds (Perovich et al., 2009). The areal fraction of melt ponds on
60 Arctic first-year ice is up to 53% and 20-38% on multi-year ice (e.g., Webster et al., 2015; Nicolaus
61 et al., 2012; Perovich et al., 2003; Fetterer and Untersteiner, 1998). This fraction has been shown
62 to increase from 15% to 35% for multi-year ice based on observations (Perovich et al., 2009) and
63 from 11% to 34% for the entire Arctic based on model simulations (Schröder et al., 2014). The
64 amount of radiation that is reflected back to the atmosphere is significantly reduced for melt ponds
65 compared to bare ice (e.g., Nicolaus et al., 2012). Instead, a considerable amount of radiation is

66 absorbed by and transmitted through melt ponds (e.g., Katlein et al., 2015; Nicolaus et al., 2012;
67 Ehn et al., 2011; Light et al., 2008; 2015). Consequently, the ice underlying the melt ponds warms
68 and can thin faster than bare ice during snow-free summer (Flocco et al., 2015; Hanson, 1965;
69 Untersteiner, 1961).

70 The translucent melt ponds are often considered as bright windows in Arctic sea ice, even during
71 autumn when their surface refreezes. The formation and occurrence of under-ice phytoplankton
72 blooms are highly dependent on snow and sea ice conditions and, thus, on the under-ice light field
73 (Ardyna et al., 2020). An Arctic-wide increase in the occurrence of the blooms was partly
74 explained by the increasing fraction of melt ponds (Horvat et al., 2017). Lee et al. (2015) showed
75 that ice algal masses accumulate in and under refrozen and snow-free melt ponds that favor higher
76 light availability. They argue that algal accumulations in autumn can provide an important food
77 source for higher trophic animals before and during winter.

78 This study documents a situation where a thicker snow cover accumulates on melt ponds compared
79 to bare ice after snow fall starts in autumn. The thicker snow cover reduces the light availability
80 under melt ponds to levels lower than under adjacent bare ice. Using data collected in the central
81 Arctic close to the geographic North Pole during the transition from summer to autumn in 2018,
82 we investigate the effect of snow accumulated on the refrozen melt ponds on the under-ice light
83 availability. We compare two datasets that represent the summer and autumn conditions, which
84 mainly consist of snow depth and ice thickness measurements, along with aerial images and under-
85 ice transmittance data from a remotely operated vehicle (ROV). We apply a radiative transfer
86 model to calculate an estimate for the snow accumulation threshold necessary for the light level to
87 be lower under melt ponds compared to bare ice.

88

89 **2 Materials and Methods**

90 **2.1 Study Site**

91 The data presented in this study were collected during the Arctic Ocean 2018 MOCCHA – ACAS
92 – ICE campaign (short: AO18) onboard the Swedish icebreaker *Oden*. During this campaign, a
93 temporary ice camp was set up on drifting, ponded multi-year ice close to the geographic North
94 Pole between 14 August and 14 September 2018. Snow depth, total sea ice thickness (ice thickness
95 plus snow depth) and transmitted irradiance were measured in an area of approximately 100 m x
96 100 m (Figure 1). Marker poles (M0 to M23) were deployed under the ice to facilitate ROV
97 navigation and to obtain a better co-location of the data. The mean ice thickness of bare ice was
98 1.9 m and of the ice underlying the melt ponds 1.7 m (Table S2). Melt ponds were on average 0.3
99 m deep. Here we focus on two main datasets: measurements performed between 17 and 24 August
100 represented summer conditions which were characterized by open or only slightly refrozen melt
101 ponds and no snow cover, whereas measurements performed between 13 and 14 September
102 represented autumn conditions which were characterized by refrozen and snow-covered melt
103 ponds.

104

105 **2.2 Snow Depth and Sea Ice Thickness**

106 Snow depth point measurements with a horizontal spacing of 1 to 3 m and an accuracy of 0.01 m
107 were obtained on the (pristine) study area using a Magna Probe (Snow-Hydro, Fairbanks, AK,
108 USA, Sturm and Holmgren, 2018). On snow-covered bare ice the Magna Probe likely penetrates
109 into the underlying surface scattering layer (SSL) leading to an overestimate in snow depth. The
110 GPS position of each measurement was recorded by an integrated GPS with an accuracy of 2.5 m
111 (Sturm and Holmgren, 2018).

112 Total (sea ice plus snow) thickness was determined using a ground-based electromagnetic
113 induction sounding device (GEM-2, Geophex Ltd, Raleigh, NC, USA, Hunkeler et al., 2015) using
114 the in-phase signal at a frequency of 18.33 kHz. The GEM-2 was placed on a sledge and dragged
115 across the study area in a grid pattern at the very end of the campaign. The accuracy of the total
116 thickness measurements is ± 0.1 m (Hunkeler et al., 2015). Finally, ice thickness was calculated
117 from total thickness by subtracting the (interpolated) snow depths. GPS positions of snow depth
118 and ice thickness measurements were subsequently corrected for ice drift using GPS recorders
119 placed at the acoustic transponder locations to enable co-location with the transmittance
120 measurements.

121 In addition, in situ snow depth, ice thickness, draft, freeboard, and melt pond depth were measured
122 in drill holes at the marker locations using a tape measure on 17 August.

123

124 **2.3 Under-Ice Transmittance**

125 Horizontal transects of under-ice spectral irradiance were measured by a RAMSES-ACC hyper-
126 spectral radiometer (TriOS GmbH, Rastede, Germany). The radiometer was mounted on a M500
127 ROV (Ocean Modules, Åtvidaberg, Sweden, Katlein et al., 2017). The ROV was lowered into the
128 water through a 2 x 2 m hole in the ice covered by a tent next to the study area (Figure 1).

129 The light transmittance was calculated by wavelength-integrating the transmitted irradiance from
130 350 to 920 nm and normalizing by the incident downwelling planar irradiance recorded by an
131 upward-looking reference sensor at the surface. The data were filtered for ROV pitch, roll and
132 depth, and noise was filtered from the spectra. Using the photosynthetically active radiation (400
133 to 700 nm) did not lead to qualitatively different results and conclusions in this work, and is thus
134 not further considered here.

135 For under-ice navigation, the ROV was equipped with an acoustic long baseline positioning system
136 (Pinpoint 1500 Linkquest, San Diego, CA, USA). We manually post-processed the ROV position
137 to remove distortions caused by calibration uncertainties.

138

139 **2.4 Aerial Images**

140 Oblique aerial images were obtained during a helicopter flight on 23 August (summer) and by a
141 drone on 13 September (autumn). Those were used to retrieve the geographic coordinates of the
142 melt ponds. The images were corrected for camera perspective and georeferenced using the marker
143 locations measured by a terrestrial laser scanner (VZ-400i, RIEGL, Horn, Austria). Melt ponds in
144 the image were detected using a simple threshold criterion. All pixels within the study area where
145 $\text{mean}(R,G,B) < 70 + 0.5 \cdot B$ (Katlein et al., 2015) were classified as melt ponds, with R, G, B
146 representing the integer values of the respective channels of the RGB color space (R=700 nm,
147 G=525 nm, B=450 nm). We added a 2 m buffer by image dilation to account for horizontal light
148 spreading (Ehn et al., 2011) and uncertainties of the ROV position.

149

150 **2.5 Radiative Transfer Model**

151 We modelled broadband reflection and under-ice transmittance using the radiative transfer model
152 DORT2002 version 3.0 (Edström, 2005; Katlein et al., 2021). The model uses a discrete ordinate
153 model geometry and is implemented in the MATLABTM software. The ice geometry was
154 approximated by three layers each for bare ice and melt ponds (Table S1): The bare ice consisted
155 of the interior sea ice underlying a SSL with a freshly fallen snow layer of varying thickness on
156 top. The melt ponds consisted of interior sea ice underlying the melt pond overlain by a snow layer
157 of varying thickness. For simplicity, the situation without any snow will be referred to as “summer”

158 conditions whereas the snow covered scenario is referred to as “autumn” conditions. We used
 159 typical inherent optical properties for multi-year ice (Katlein et al., 2021; Perron et al., 2021).

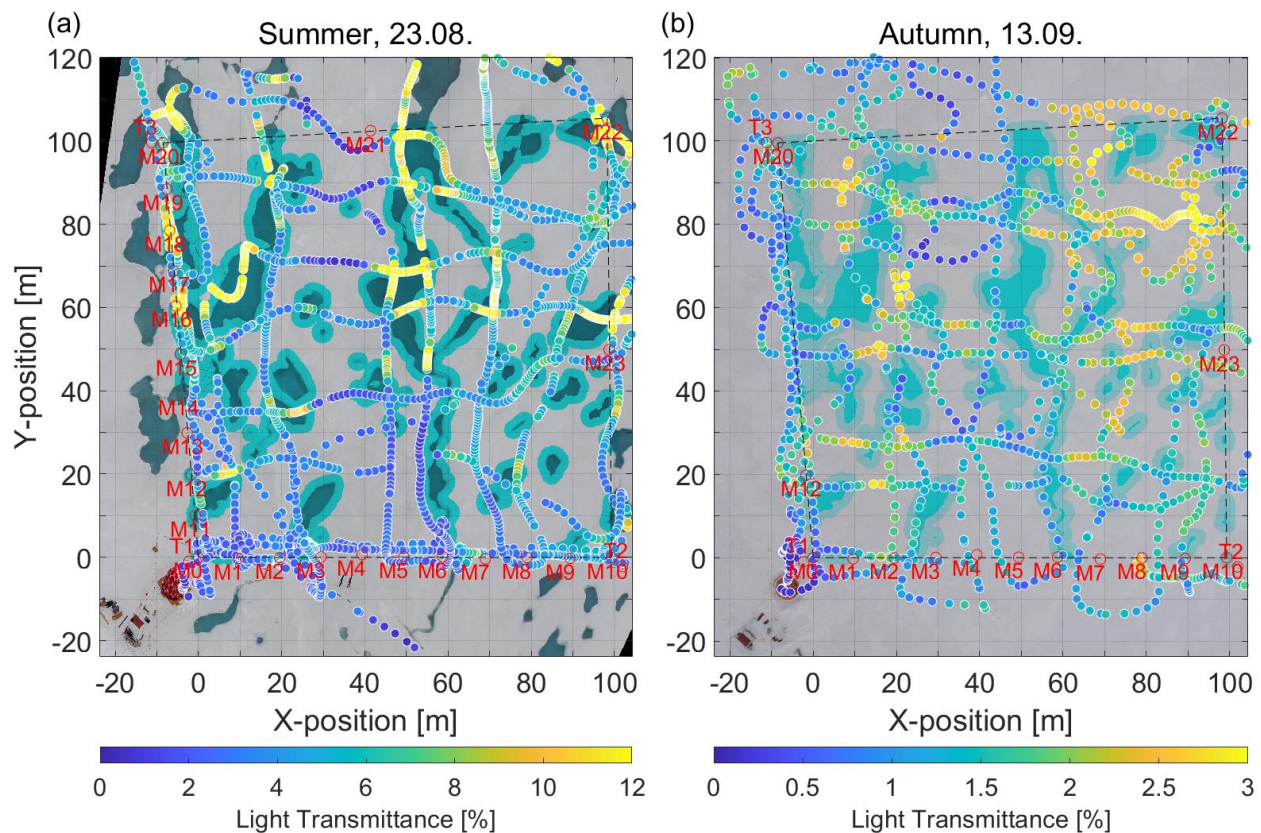
160

161 3 Results and Discussion

162 3.1 Evolution of the Snow Cover in the Transition from Summer to Autumn

163 Figure 1 illustrates the distribution of melt ponds and bare ice and their surface properties during
 164 the transition from summer to autumn in the study area.

165



166

167 **Figure 1:** Light transmittance through ponded sea ice during the transition from (a) summer to (b)
 168 autumn. The data show ROV-based radiation measurements under (a) open melts ponds and (b)
 169 refrozen and snow-covered ponds. The background images are orthorectified aerial images
 170 acquired during (a) a low altitude helicopter flight and (b) a drone flight. Pixels within the study

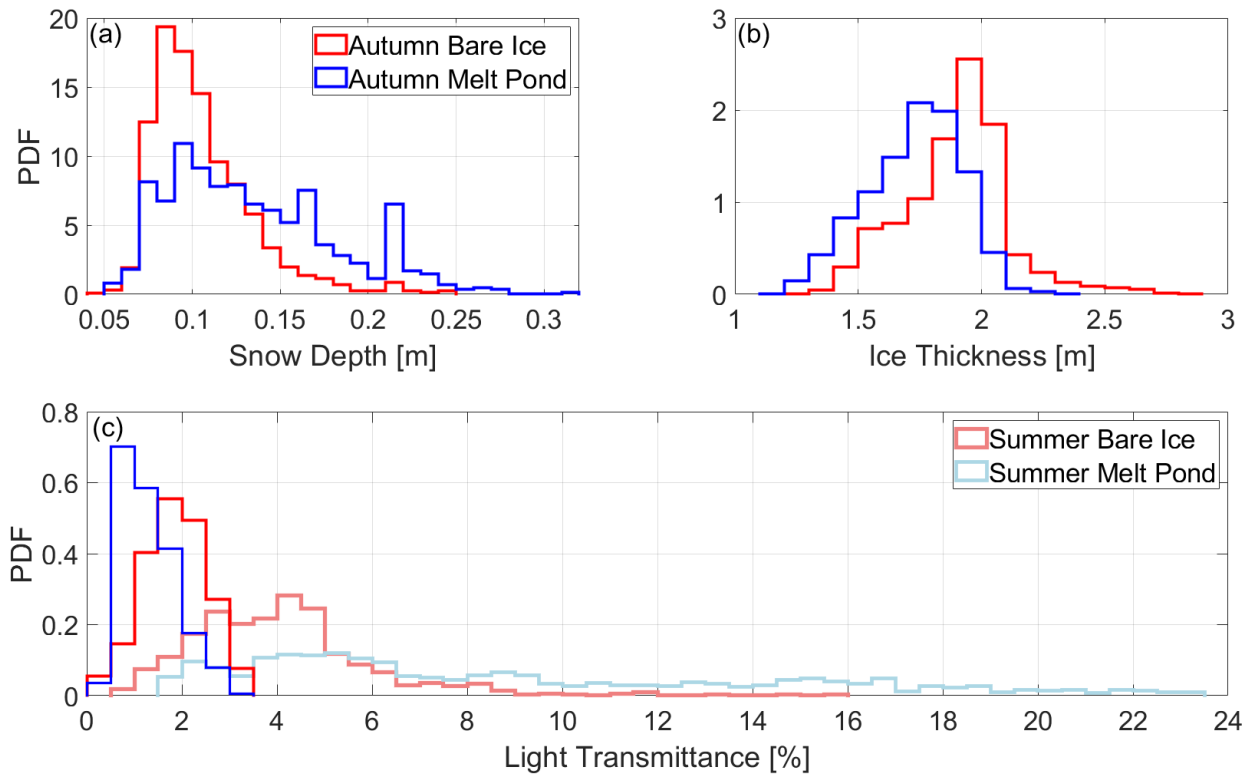
171 area that were classified as melt pond and used for further analysis are colored in blue. The melt
172 ponds in (b) were refrozen and snow-covered but marked blue for illustration purposes. The edges
173 around the melt ponds in (a) and (b) were dilated by a buffer of about 2 m. This area is indicated
174 by a brighter blue. Red labels indicate the marker (M) and transponder locations (T). The ROV
175 tent and control hut are visible on the lower left corners of the images. Note the different range in
176 transmittance in (a) and (b).

177

178 On 23 August, the melt ponds were generally still open but in parts slightly refrozen at the surface
179 (Figures 1a and S1). No significant snow fall occurred prior to 29 August (Vüllers et al., 2019),
180 however a SSL of deteriorated ice with a mean thickness of 0.07 m was present. The passage of
181 low-pressure systems between 29 August and 15 September brought precipitation accompanied
182 by strong winds with speeds up to 13 ms^{-1} (Vüllers et al., 2019). This wind speed exceeded the
183 threshold of $8\text{-}10 \text{ ms}^{-1}$ under which divergence of large amounts of drifting snow is favourable
184 (Van den Broeke and Bintanja, 1995). As a result, snow was deposited and re-distributed towards
185 and caught by the recessed and refrozen melt ponds and their edges (Figure S1, Fetterer &
186 Untersteiner, 1998; Perovich et al., 2003). This led to a higher mean snow accumulation on the
187 ponds (0.14 m) compared to on bare ice (0.11 m) as measured on 13 September (Figure 2a, Table
188 S2). On the melt ponds, higher snow depths were also much more frequently measured than on
189 bare ice (modes of 0.17 and 0.22 m, Figure 2a).

190 The snow mostly covered the visible surface signature of the ponds (Figure 1). However, the ponds
191 were still discernible because of their brighter appearance due to the higher snow depth compared
192 to the adjacent bare ice (Figure 1b).

193



194

195 **Figure 2:** Histograms of measured (a) snow depth, (b) ice thickness, and (c) light transmittance of
 196 melt ponds and bare ice.

197

198 The higher snow depth on the melt ponds can have important implications on the sea ice mass
 199 balance related to the insulating effect of the snow cover (Sturm et al., 1997). Reduced heat loss
 200 (Maykut, 1978) and thermodynamic ice growth (Merkouriadi et al., 2017; Maykut, 1978) as well
 201 as delayed freeze-up of the liquid melt pond (Flocco et al., 2015) and induced bottom roughness
 202 are expected.

203 The refrozen surface of the melt ponds alone reduces the heat release from the ocean through the
 204 ice towards the atmosphere (Flocco et al., 2015). This hampers ice growth at both water-ice
 205 interfaces of the refreezing pond, as well as between the sea ice bottom and the ocean in the
 206 transition from autumn to winter. This can result in a delay of the complete freeze-up of the pond
 207 by up to 60 days (Flocco et al., 2015). A thinner ice cover is more vulnerable to dynamic and

208 warming events. The presence of a snow cover on top of the refrozen pond surface and the still
209 liquid melt pond underneath are expected to amplify those effects (Perovich et al., 2003). As a
210 result of the reduced thermodynamic growth of the sea ice underlying melt ponds compared to
211 bare ice, a generally rougher bottom topography might result, affecting the mass, momentum, heat,
212 and salt fluxes at the sea ice-ocean interface.

213 The exact evolution of the thicker snow cover on melt ponds during refreezing depends on the
214 sequence of weather events. Whether or not more snow accumulates on the refrozen melt ponds
215 than on adjacent bare ice is governed by the wind speed and snow drift regime during and after the
216 snow fall, by the snow properties, and by the roughness of the refrozen surface. Falling and
217 deposited snow needs to be re-distributed before it can accumulate on the topographically recessed
218 and rougher pond surface. Wet and heavy snow is more resistant to erosion by wind than low-
219 density dry snow (e.g., Colbeck, 1979; Massom et al., 1997). For instance, new snow deposited on
220 blue ice either by drifting or precipitation can hardly settle on the smooth and warm-temperate
221 surface (Bintanja, 1999; Van den Broeke and Bintanja, 1995). In case downwind slopes are
222 smooth, any snow that can temporarily accumulate is prevented from actually attaching to the
223 surface (Dadic et al., 2013; Bintanja, 1999). On such surfaces, drifting snow is also prevented from
224 becoming attached causing the wind to be stronger over the glazed surface than over the snow
225 (Ferzzotti et al., 2002a). Furthermore, less snow will accumulate on smooth nilas with a low
226 surface roughness (e.g., Sturm et al., 2002; Massom et al., 1997) than on surfaces with a higher
227 surface roughness (e.g., Bintanja, 1999, Frezzotti, 2002b).

228

229 **3.2 Optical Properties**

230 The surface topography of the ponded ice cover was key in modulating spatial variability in snow
231 depth and hence light transmittance: The presence of open melt ponds in summer and the
232 variability in snow depth driven by the refrozen melt ponds in autumn also led to spatial and
233 temporal variability in the under-ice light field. On 24 August, ROV-based mean and maximum
234 transmittances of ponds (8.9% and 23.2%, respectively) were significantly higher than those of
235 bare ice (4.1% and 15.5%, see also Figures 1a and 2c and Table S2). Histograms showed a bi-
236 modal transmittance distribution of ponds and bare ice combined (Figure S2). The distribution also
237 showed a characteristic long tail for ponds, indicating high spatial variability and different
238 properties of the ponds. This distribution is typical for Arctic summer sea ice and results from the
239 formation and development of the melt ponds (Katlein et al., 2015; 2019; Nicolaus et al., 2012;
240 Schanke et al., 2021). The magnitudes of transmittance are similar to observations from Nicolaus
241 et al. (2012) in the same region in August 2011. The maximum transmittance of the melt ponds
242 also agrees to values found by Katlein et al. (2019).

243
244 Due to the new snow cover on top of both the refrozen melt ponds and the bare ice (Figure 1b),
245 the transmittance of both melt ponds and bare ice decreased (Figures 1 and S2, Table S2). The
246 spatial variability in the transmittance of both melt ponds and bare ice was significantly reduced
247 in autumn while the long tail of the high transmittances diminished, with very few observations
248 higher than 3% (Figures 2c and S2, Table S2). In summer, approximately 80% (25%) of the
249 transmittance measurements were higher than 3% (9%). Due to stronger and more frequent snow
250 fall events that started to occur from 28 August (Vüllers et al., 2021), only 1% (0%) of the
251 transmittances measurements in autumn were higher than 3% (9%).

252 Lee et al. (2011) describe observations indicating that melt ponds remain bright windows even in
253 autumn after refreezing, although they did not consider a snow cover. This implies that the
254 transmittance of melt ponds remains higher than that of bare ice. Katlein et al. (2019) showed that
255 the bi-modal structure of transmittance during summer is conserved even during the first weeks of
256 freeze-up in mid of September. They further suggest that the transmittances of both melt ponds
257 and bare ice decrease gradually and equally in the transition from summer to autumn. Snow and
258 particular re-distribution were present during their transmittance measurements, however those
259 were not adequately considered.

260 We observed a different scenario than Lee et al. (2011) and Katlein et al. (2019). A thicker snow
261 cover accumulated on melt ponds compared to adjacent bare ice because of the pond's recessed
262 topography. This led to a lower mean transmittance of melt ponds (1.3%) than of bare ice (1.8%)
263 in autumn (Figures 1 and 2c, Table S2). The transmittance distribution showed two distinct modes
264 of 1.0% and 2.0% associated with melt ponds and bare ice, respectively (Figure 2c, Table S2).

265 Despite the reversal of the magnitude in the transmittance of melt ponds and bare ice, the spatial
266 variability remained during autumn (Figure 1). This suggests that the spatial variability was still
267 coupled to the ponds after snow accumulation and re-distribution and most likely also persisted
268 into winter.

269 The transmittance of ridged ice with thicknesses up to 2.8 m was naturally still lower than that of
270 the melt ponds (Figures S3b and 1b). Those measurements are included in the bare ice data and
271 are represented in the tail of larger ice thicknesses in the histogram (Figure 2b).

272 This study provides first quantitative observations of lower light transmittance of melt ponds than
273 of bare ice in autumn due to higher snow depths on the ponds. Major implications on the ice-

274 associated ecosystem and the energy balance of the sea ice might arise from those observations in
275 case such a situation is viable for the entire Arctic which is very likely:

276 Lee et al. (2011) proposed that the soft refrozen surface of open melt ponds that are in connection
277 with the ocean provides a fertile habitat for biomass in autumn. They pointed out that the biomass
278 accumulated under the refrozen melt ponds serves as an important food source for higher trophic
279 animals during the transition from autumn to winter and further into winter. However, as presented
280 here, a snow cover significantly reduces the light availability in and under melt ponds in autumn,
281 suggesting a limited suitability as habitat in terms of available light. Those observations lend
282 support to a study by Lange et al. (2017), who found higher biomass values underneath hummocks
283 on multi-year ice compared to adjacent level ice. Lange et al. (2017) attributed the differences in
284 biomass accumulation to increased light availability under the hummocks resulting from a very
285 thin or absent snow cover (Perovich et al., 2003). Our results and those of Lange et al. (2017)
286 suggest that light conditions under sea ice in spring can already be initialized by melt pond
287 coverage and snow distribution during autumn and may persist throughout winter.

288 Further, due to the common assumption that there is more light available under melt ponds than
289 under bare ice also during autumn, processes and magnitudes of carbon uptake and biomass
290 accumulation in models, might need to be adjusted with respect to our new observations.

291 Arndt and Nicolaus (2014) developed a parameterization to quantify the annual solar heat input
292 through Arctic sea ice. For their calculations in autumn, they use for transmittances of melt ponds
293 the fivefold (500%) of that of bare ice. However, our results showed that the modal transmittance
294 of melt ponds is only half (50%) of that of bare ice once covered by the first snow (Table S2).
295 Arndt and Nicolaus (2014) applied a constant summer mean melt pond fraction for multi-year ice
296 of 29% (Rösel et al., 2012) and a transmittance of melt ponds for multi-year ice of 0.4%. They

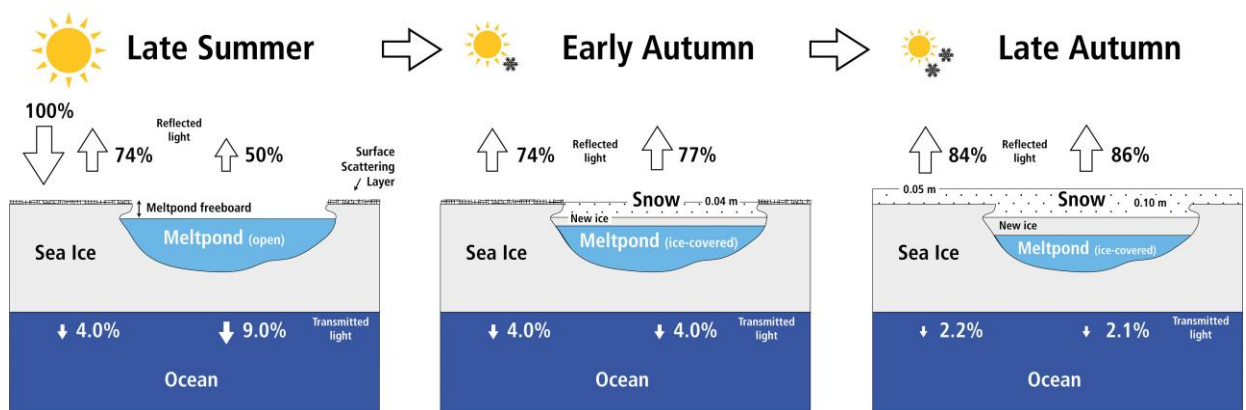
297 estimated the solar heat input into the ocean in September to 0.69×10^{19} J. We adopted their
 298 parameters but used the ratio of transmittances between melt ponds and bare ice as presented in
 299 the present study. As a result, the solar heat input into the ocean decreased by 61%. This shows,
 300 that despite the generally low solar energy fluxes in autumn compared to in summer (e.g., Perovich
 301 et al., 2011; Arndt and Nicolaus, 2014), our described effect could have an important impact on
 302 the energy budget if valid in the entire Arctic. In this regard, our results might also impact the
 303 heat stored in the upper ocean, the interior sea ice structure, as well as internal and basal melting.

304

305 3.3 Radiative Transfer Model

306 For the effect described above, it is of interest to quantify the threshold snow depth that is necessary
 307 to decrease the transmittance of melt ponds below that of bare ice. In order to determine this
 308 threshold depth, we used the radiative transfer model DORT2002. Figure 3 summaries the
 309 observations of this study in a schematic which are supported by simulated albedo and
 310 transmittance. For the situation without snow (summer), both the simulated transmittances of melt
 311 ponds and bare ice (9% and 4%, respectively) were very similar to our observations (8.9% and
 312 4.1%, respectively, Figures 3 and S4, Table S2).

313



314

315 **Figure 3:** Simulated reflected light (albedo) and transmitted light (transmittance) as a function of
316 snow depth as modelled by DORT2002 for (left) snow-free melt ponds and bare ice, (middle)
317 snow-covered melt ponds and snow-free bare ice, and (right) snow-covered melt ponds and bare
318 ice. Properties used in the model are display in Table S1.

319

320 Incorporating an increasing snow cover from 0 to 0.20 m (autumn), our results yielded an
321 exponential decrease in the transmittances of both melt ponds and bare ice (Figure S4). For a snow
322 depth of approximately 0.04 m the transmittance of the melt ponds becomes equal to that of snow-
323 free bare ice (Figures 3 and S4). This is in agreement with the observations presented earlier which
324 showed that the transmittance of melt ponds was lower than that of bare ice for a 0.03 m higher
325 mean snow depth on the ponds (Table S2). Figure 3c illustrates that the transmittance of melt ponds
326 with a 0.10 m thick snow cover becomes lower than that of bare ice with a 0.05 m thick snow
327 cover.

328 In our simulations, the influence of the thin ice lid on the melt ponds on the transmittance was
329 neglected, as they were only partially existing, as for typical Arctic summer sea ice these are very
330 translucent and scattering is small (Lu et al., 2018), indicated by their blue-green color (Figure 1a).

331

332 **5 Summary**

333 Snow depth measurements on a ponded sea ice floe in the transition from summer to autumn reveal
334 that snow accumulation was on average 0.03 m higher on refrozen melt ponds than on adjacent
335 bare ice favored by the ponds recessed surface. Using under-ice radiation measurements from a
336 ROV we show that due to the thicker snow cover on the melt ponds the transmittance of the melt
337 ponds can become lower than that of bare ice. Those results imply that melt ponds cannot be

338 universally considered as bright windows of Arctic autumn sea ice. Computations from a radiative
339 transfer model indicate that a snow cover with a depth >0.04 m accumulated on melt ponds result
340 in transmittances of melt ponds becoming lower than that of snow-free bare ice. Our findings can
341 have consequences for the autumn ecosystem activity, oceanic heat budget and thermodynamic
342 ice growth if they can be observed in the entire Arctic.

343

344 **Acknowledgments**

345 This work was financed through the research programs PACES II and POF4 of the Alfred-
346 Wegener-Institut Helmholtz-Zentrum für Polar- und Meeresforschung (AWI) and the Swedish
347 Polar Research Secretariat (SPRS, grant no. AO18). Additional funding was received through the
348 Diatom-ARCTIC project (NE/R012849/1; 03F0810A) as part of the Changing Arctic Ocean
349 program (CAO), jointly funded by the UKRI Natural Environment Research Council (NERC) and
350 the German Federal Ministry of Education and Research(BMBF). The ROV work was supported
351 by the Helmholtz Infrastructure Initiative “Frontiers in Arctic marine Monitoring” (FRAM). We
352 are thankful to the captain, crew and scientists onboard the *IB Oden*, as well as to the SPRS and
353 AWI logistics for facilitating our participation in the AO18 expedition. Our special thanks go to
354 Matthieu Labaste, Helen Czerski and Lars Lehnert for their field support, Ruzica Dadic for her
355 advice on snow, and the polar bear guarding crew for keeping us safe.

356

357 **Data availability**

358 All data presented in this study are publicly available under the following DOIs:

359 ROV: <https://doi.org/10.1594/PANGAEA.925698>

360 Magna Probe and GEM2: <https://doi.pangaea.de/10.1594/PANGAEA.934431>

361 Aerial images: <https://doi.org/10.5281/zenodo.5119094>

362

363 **Competing interest**

364 The authors declare that they have no conflict of interest.

365

366 **References**

- 367 Ardyna, M., Mundy, C. J., Mills, M. M., Oziel, L., Grondin, L. L., Verin, G., et al. (2020).
368 Environmental drivers of under-ice phytoplankton bloom dynamics in the Arctic Ocean.
369 *Elementa: Science of the Anthropocene*, 8(30). doi:10.1525/elementa.430
- 370 Arndt, S., & Nicolaus, M. (2014). Seasonal cycle and long-term trend of solar energy fluxes
371 through Arctic sea ice. *The Cryosphere*, 8(6). doi:10.5194/tc-8-2219-2014
- 372 Arrigo, K. R. (2014). Sea ice ecosystems. *Annual Review of Marine Science*, 6(1).
373 doi:10.1146/annurev-marine-010213-135103
- 374 Bintanja, R. (1999). On the glaciological, meteorological, and climatological significance of
375 Antarctic blue ice areas. *Reviews of Geophysics*, 37(3). doi:10.1029/1999rg900007
- 376 Colbeck, S. C. (1979). Sintering and compaction of snow containing liquid water. *Philosophical
377 Magazine A*, 39(1). doi:10.1080/01418617908239272
- 378 Dadic, R., Mott, R., Horgan, H. J., & Lehning, M. (2013). Observations, theory, and modeling of
379 the differential accumulation of Antarctic megadunes. *Journal of Geophysical Research:
380 Earth Surface*, 118(4). doi:10.1002/2013jf002844
- 381 Edström, P. (2005). A Fast and Stable Solution Method for the Radiative Transfer Problem. *SIAM
382 Rev.*, 47(3). doi:10.1137/s0036144503438718
- 383 Ehn, J. K., Papakyriakou, T. N., & Barber, D. G. (2008). Inference of optical properties from
384 radiation profiles within melting landfast sea ice. *Journal of Geophysical Research*,
385 113(C09024). doi:10.1029/2007jc004656
- 386 Ehn, J. K., Mundy, C. J., Barber, D. G., Hop, H., Rossnagel, A., & Stewart, J. (2011). Impact of
387 horizontal spreading on light propagation in melt pond covered seasonal sea ice in the
388 Canadian Arctic. *Journal of Geophysical Research*, 116. doi:10.1029/2010jc006908
- 389 Fetterer, F., & Untersteiner, N. (1998). Observations of melt ponds on Arctic sea ice. *Journal of
390 Geophysical Research: Oceans*, 103(C11). doi:10.1029/98jc02034
- 391 Frezzotti, M., Gandolfi, S., & Urbini, S. (2002a). Snow megadunes in Antarctica: Sedimentary
392 structure and genesis. *Journal of Geophysical Research*, 107(D18).
393 doi:10.1029/2001jd000673
- 394 Frezzotti, M., Gandolfi, S., La Marca, F., & Urbini, S. (2002b). Snow dunes and glazed surfaces
395 in Antarctica: new field and remote-sensing data. *Annals of Glaciology*, 34.
396 doi:10.3189/172756402781817851
- 397 Flocco, D., Feltham, D. L., Bailey, E., & Schroeder, D. (2015). The refreezing of melt ponds on
398 Arctic sea ice. *Journal of Geophysical Research: Oceans*, 120(2).
399 doi:10.1002/2014jc010140

- 400 Grenfell, T. C., & Maykut, G. A. (1977). The optical properties of ice and snow in the Arctic
401 Basin. *Journal of Glaciology*, 18(80). doi:10.3189/S0022143000021122
- 402 Hanson, A. (1965). Studies of the Mass Budget of Arctic Pack-Ice Floes. *Journal of Glaciology*,
403 5(41). doi:10.3189/S0022143000018694
- 404 Hunkeler, P. A., Hoppmann, M., Hendricks, S., Kalscheuer, T., & Gerdes, R. (2016). A glimpse
405 beneath Antarctic sea ice: Platelet layer volume from multifrequency electromagnetic
406 induction sounding. *Geophysical Research Letters*, 43(1). doi:10.1002/2015gl065074
- 407 Katlein, C., Arndt, S., Nicolaus, M., Perovich, D. K., Jakuba, M. V., Suman, S., et al. (2015).
408 Influence of ice thickness and surface properties on light transmission through Arctic sea
409 ice. *Journal of Geophysical Research: Oceans*, 120(9). doi:10.1002/2015JC010914
- 410 Katlein, C., Schiller, M., Belter, H. J., Coppolaro, V., Wenslandt, D., & Nicolaus, M. (2017). A
411 New Remotely Operated Sensor Platform for Interdisciplinary Observations under Sea Ice.
412 *Frontiers in Marine Science*, 4. doi:10.3389/fmars.2017.00281
- 413 Katlein, C., Arndt, S., Belter, H. J., Castellani, G., & Nicolaus, M. (2019). Seasonal Evolution of
414 Light Transmission Distributions Through Arctic Sea Ice. *Journal of Geophysical
415 Research: Oceans*, 124(8). doi:10.1029/2018jc014833
- 416 Katlein, C., Valcic, L., Lambert-Girard, S., & Hoppmann, M. (2021). New insights into radiative
417 transfer within sea ice derived from autonomous optical propagation measurements. *The
418 Cryosphere*, 15(1). doi:10.5194/tc-15-183-2021
- 419 Lange, B. A., Flores, H., Michel, C., Beckers, J. F., Bublit, A., Casey, J. A., et al. (2017). Pan-
420 Arctic sea ice-algal chl a biomass and suitable habitat are largely underestimated for
421 multiyear ice. *Global Change Biology*, 23(11). doi:10.1111/gcb.13742
- 422 Lee, S. H., McRoy, C. P., Joo, H. M., Gradinger, R., Cui, H., Yun, M. S., et al. (2011). Holes in
423 Progressively Thinning Arctic Sea Ice Lead to New Ice Algae Habitat. *Oceanography*,
424 24(3). doi:10.5670/oceanog.2011.81
- 425 Light, B., Grenfell, T. C., & Perovich, D. K. (2008). Transmission and absorption of solar radiation
426 by Arctic sea ice during the melt season. *Journal of Geophysical Research*, 113(C03023).
427 doi:10.1029/2006jc003977
- 428 Light, B., Perovich, D. K., Webster, M. A., Polashenski, C., & Dadic, R. (2015). Optical properties
429 of melting first-year Arctic sea ice. *Journal of Geophysical Research: Oceans*, 120(11).
430 doi:10.1002/2015jc011163
- 431 Lu, P., Cao, X., Wang, Q., Leppäranta, M., Cheng, B., & Li, Z. (2018). Impact of a Surface Ice
432 Lid on the Optical Properties of Melt Ponds. *Journal of Geophysical Research: Oceans*,
433 123(11). doi:10.1029/2018jc014161
- 434 Massom, R. A., Drinkwater, M. R., & Haas, C. (1997). Winter snow cover on sea ice in the
435 Weddell Sea. *Journal of Geophysical Research: Oceans*, 102(C1). doi:10.1029/96jc02992
- 436 Maykut, G. A. (1978). Energy exchange over young sea ice in the central Arctic. *Journal of
437 Geophysical Research*, 83(C7). doi:10.1029/JC083iC07p03646
- 438 Merkouriadi, I., Cheng, B., Graham, R. M., Rösel, A., & Granskog, M. A. (2017). Critical Role of
439 Snow on Sea Ice Growth in the Atlantic Sector of the Arctic Ocean. *Geophysical Research
440 Letters*, 44(20). doi:10.1002/2017gl075494
- 441 Nicolaus, M., Katlein, C., Maslanik, J., & Hendricks, S. (2012). Changes in Arctic sea ice result
442 in increasing light transmittance and absorption. *Geophysical Research Letters*, 39(24).
443 doi:10.1029/2012gl053738

- 444 Perovich, D. K. (1990). Theoretical estimates of light reflection and transmission by spatially
445 complex and temporally varying sea ice covers. *Journal of Geophysical Research*, *95*(C6).
446 doi:10.1029/JC095iC06p09557
- 447 Perovich, D. K., Tucker III, W. B., & Ligett, K. A. (2002). Aerial observations of the evolution of
448 ice surface conditions during summer. *Journal of Geophysical Research*, *107*(C10).
449 doi:10.1029/2000jc000449
- 450 Perovich, D. K., Grenfell, T. C., Richter-Menge, J. A., Light, B., Tucker III, W. B., & Eicken, H.
451 (2003). Thin and thinner: Sea ice mass balance measurements during SHEBA. *Journal of*
452 *Geophysical Research*, *108*(C3). doi:10.1029/2001jc001079
- 453 Perovich, D. K., Grenfell, T. C., Light, B., Elder, B. C., Harbeck, J. P., Polashenski, C., et al.
454 (2009). Transpolar observations of the morphological properties of Arctic sea ice. *Journal*
455 *of Geophysical Research*, *114*(C00A04). doi:10.1029/2008jc004892
- 456 Perovich, D. K., Richter-Menge, J. A., Jones, K. F., Light, B., Elder, B. C., Polashenski, C., et al.
457 (2011). Arctic sea-ice melt in 2008 and the role of solar heating. *Annals of Glaciology*,
458 *52*(57). doi:10.3189/172756411795931714
- 459 Perron, C., Katlein, C., Lambert-Girard, S., Leymarie, E., Guinard, L.-P., Marquet, P., et al. (2021).
460 Development of a Diffuse Reflectance Probe for In Situ Measurement of Inherent Optical
461 Properties in Sea Ice, *The Cryosphere Discuss.*, in review, doi:10.5194/tc-2021-104
- 462 Petrich, C., Eicken, H., Polashenski, C. M., Sturm, M., Harbeck, J. P., Perovich, D. K., et al.
463 (2012a). Snow dunes: A controlling factor of melt pond distribution on Arctic sea ice.
464 *Journal of Geophysical Research: Oceans*, *117*(C09029). doi:10.1029/2012jc008192
- 465 Petrich, C., Nicolaus, M., & Gradinger, R. (2012b). Sensitivity of the light field under sea ice to
466 spatially inhomogeneous optical properties and incident light assessed with three-
467 dimensional Monte Carlo radiative transfer simulations. *Cold Regions Science and*
468 *Technology*, *73*. doi:10.1016/j.coldregions.2011.12.004
- 469 Polashenski, C., Perovich, D. K., & Courville, Z. (2012). The mechanisms of sea ice melt pond
470 formation and evolution. *Journal of Geophysical Research: Oceans*, *117*(C1).
471 doi:10.1029/2011jc007231
- 472 Rösel, A., Kaleschke, L., & Birnbaum, G. (2012). Melt ponds on Arctic sea ice determined from
473 MODIS satellite data using an artificial neural network. *The Cryosphere*, *6*(2).
474 doi:10.5194/tc-6-431-2012
- 475 Schröder, D., Feltham, D. L., Flocco, D., & Tsamados, M. (2014). September Arctic sea-ice
476 minimum predicted by spring melt-pond fraction. *Nature Climate Change*, *4*(5).
477 doi:10.1038/nclimate2203
- 478 Sturm, M., Holmgren, J., König, M., & Morris, K. (1997). The thermal conductivity seasonal
479 snow. *Journal of Glaciology*, *43*(143). doi:10.3189/S0022143000002781
- 480 Sturm, M., Holmgren, J., & Perovich, D. K. (2002). Winter snow cover on the sea ice of the Arctic
481 Ocean at the Surface Heat Budget of the Arctic Ocean (SHEBA): Temporal evolution and
482 spatial variability. *Journal of Geophysical Research*, *107*(C10).
483 doi:10.1029/2000jc000400
- 484 Sturm, M., & Holmgren, J. (2018). An Automatic Snow Depth Probe for Field Validation
485 Campaigns. *Water Resources Research*, *54*(11). doi:10.1029/2018wr023559
- 486 Untersteiner, N. (1961). On the Mass and Heat Budget of Arctic Sea Ice. *Archiv für Meteorologie,*
487 *Geophysik und Bioklimatologie, Serie A*, *12*. doi:10.1007/BF02247491

- 488 Van den Broeke, M., & Bintanja, R. (1995). Summertime Atmospheric Circulation in the Vicinity
489 of a Blue Ice Area in Queen Maud Land, Antarctica. *Boundary-Layer Meteorology*, 72(4).
490 doi:10.1007/BF00709002
- 491 Vüllers, J., Achtert, P., Brooks, I. M., Tjernström, M., Prytherch, J., Burzik, A., et al. (2021).
492 Meteorological and cloud conditions during the Arctic Ocean 2018 expedition.
493 *Atmospheric Chemistry and Physics*, 21(1). doi:10.5194/acp-21-289-2021
- 494 Webster, M. A., Rigor, I. G., Nghiem, S. V., Kurtz, N. T., Farrell, S. L., Perovich, D. K., et al.
495 (2014). Interdecadal changes in snow depth on Arctic sea ice. *Journal of Geophysical*
496 *Research: Oceans*, 119(8). doi:10.1002/2014jc009985
- 497 Webster, M. A., Rigor, I. G., Perovich, D. K., Richter-Menge, J. A., Polashenski, C. M., & Light,
498 B. (2015). Seasonal evolution of melt ponds on Arctic sea ice. *Journal of Geophysical*
499 *Research: Oceans*, 120(9). doi:10.1002/2015jc011030
- 500 Webster, M. A., Gerland, S., Holland, M. M., Hunke, E., Kwok, R., Lecomte, O., et al. (2018).
501 Snow in the changing sea-ice systems. *Nature Climate Change*, 8(11).
502 doi:10.1038/s41558-018-0286-7
503

Geophysical Research Letters

Supporting Information for

**From Bright Windows to Dark Spots: Snow Cover Controls Melt Pond Optical
Properties During Refreezing**

P. Anhaus^{1*}, C. Katlein¹, M. Nicolaus¹, M. Hoppmann¹, C. Haas^{1,2}

¹Alfred-Wegener-Institut Helmholtz-Zentrum für Polar- und Meeresforschung,
Bremerhaven, Germany

²Department of Environmental Physics, University of Bremen, Bremen, Germany

*Corresponding author: Philipp Anhaus (philipp.anhaus@awi.de)

Contents of this file

Figures S1 to S4

Tables S1 to S2



Figure S1: Photograph as of 23 August illustrating that refrozen melt ponds have a recessed topographic position within the adjacent bare ice.

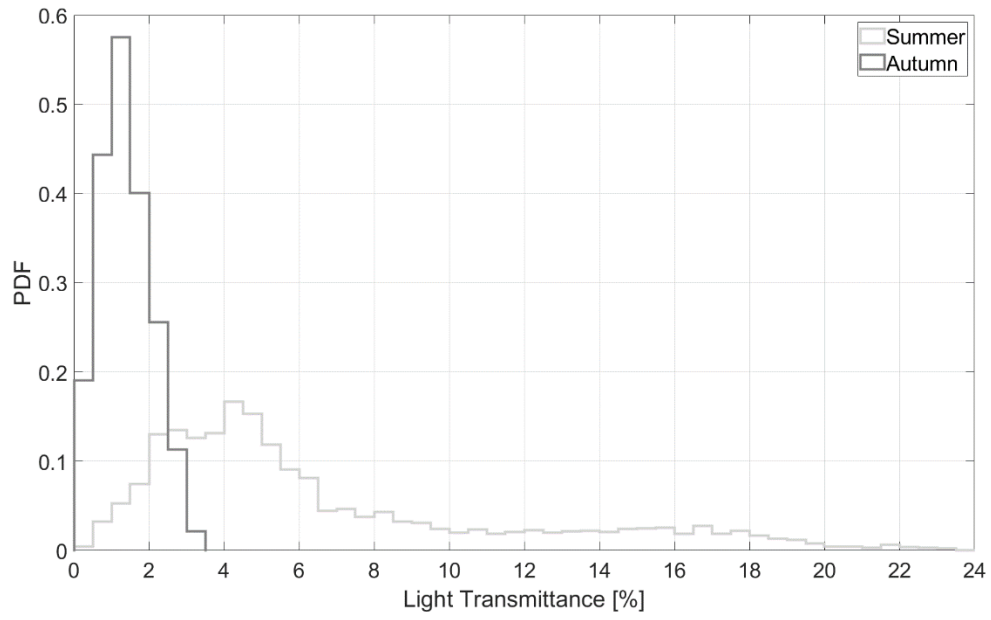


Figure S2: Histograms of light transmittance as measured on 24 August (summer) and 13 September (autumn) of melt ponds and bare ice combined.

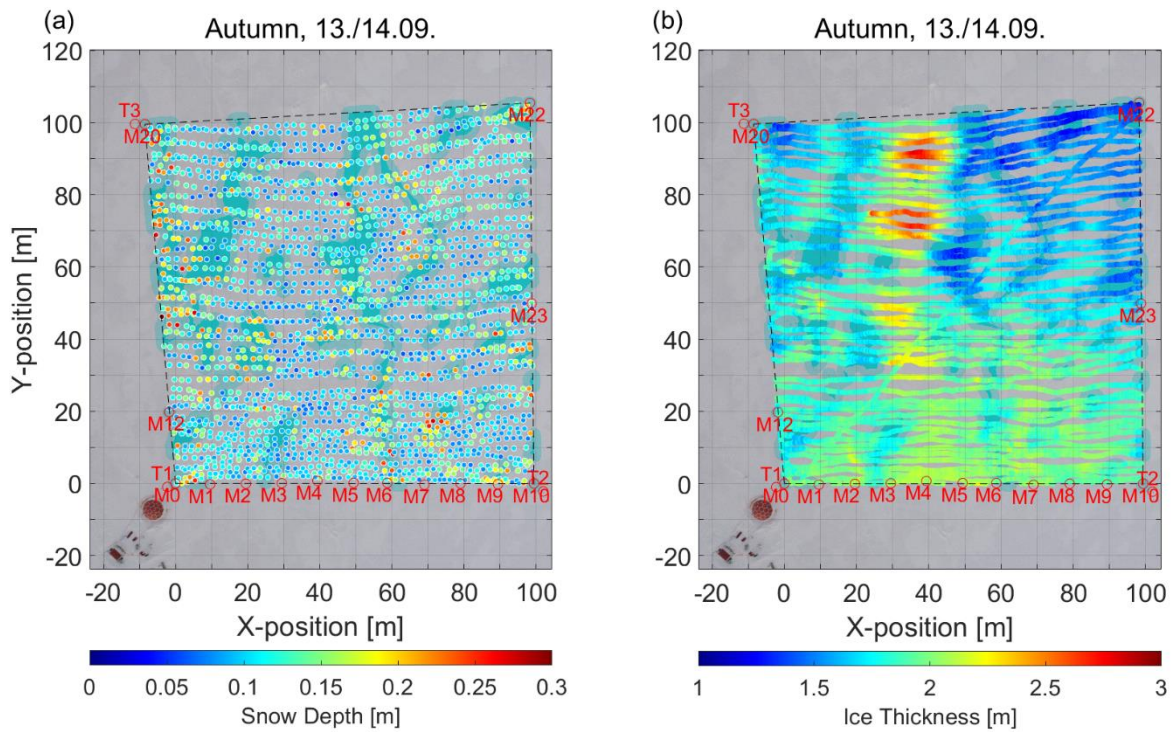


Figure S3: (a) Snow depth and (b) ice thickness on ponded sea ice as measured on 14 September (autumn). The background images are orthorectified aerial images acquired during a drone flight on 13 September. Pixels within the area of focus that were classified as melt pond during the summer are colored in light blue to illustrate the refrozen and snow-covered ponds during autumn. The edges around the melt ponds were dilated by a buffer of about 2 m. This area is indicated by a brighter blue. Red labels indicate the marker (M) and transponder locations (T). The ROV tent and control hut are visible on the lower left corners of the images.

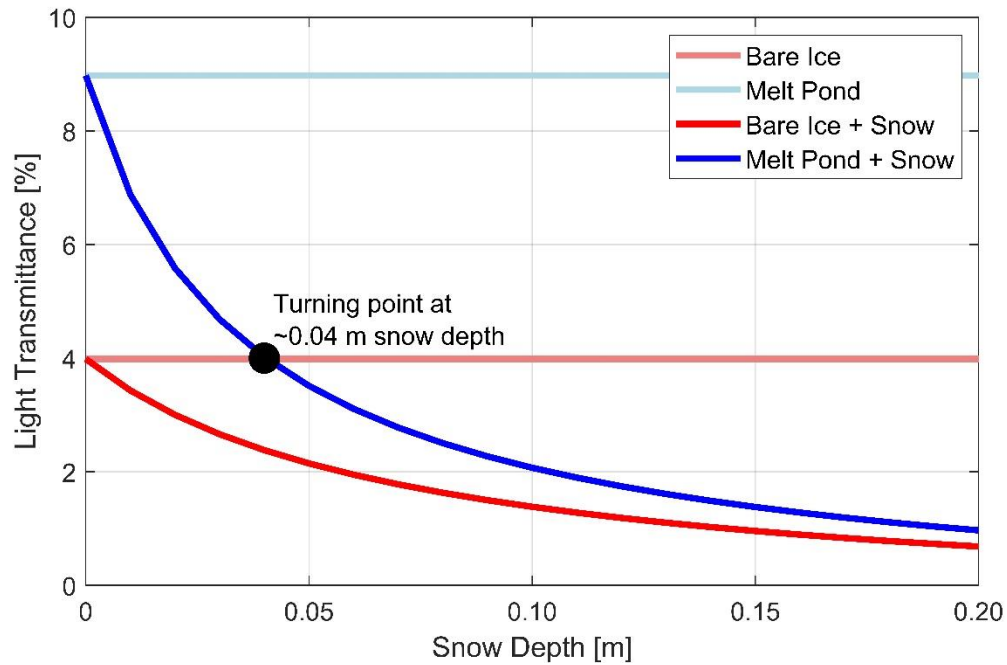


Figure S4: Simulated light transmittance depending on the snow depth as modelled by DORT2002 for four cases: bare ice (light red), melt ponds (light blue), snow-covered bare ice (red), and snow-covered melt ponds (blue).

Table S1: Parameters used in the radiative transfer model. SSL is the surface scattering layer. The melt pond depth is based on the in-situ average melt pond depth measured at six marker locations. The scattering coefficient for cold dry snow was provided by Perovich (1990). The other parameters were chosen with respect to Ehn et al. (2008), Light et al. (2008), Petrich et al. (2012b), and Katlein et al. (2021) and adjusted so that they resulted in transmittance values similar to our observations. A Henyey–Greenstein phase function with an asymmetry parameter $g = 0.9$ was used for all layers.

Type	Layer Thickness [m]		Scattering Coefficient [m ⁻¹]	Absorption Coefficient [m ⁻¹]	Refractive Index
	Bare	Pond			
<hr/>					

Snow	0 - 0.2	0 - 0.2	800	0.15	1.33
SSL	0.1	-	250	0.15	1.33
Interior ice	2.0	1.8	25	0.15	1.33
Pond	-	0.3	0	0.10	1.30

Table S2: Statistics of measured snow depth (m), ice thickness (m), and light transmittance (%), of melt ponds and bare ice. N is the number of measurements. The modes were read from histograms (Figure 2) with bin widths of 0.01 m, 0.10 m, and 0.5 %, respectively.

Variable	Date	Type	N	Min	Max	Mean	Std	Median	Mode
Snow Depth [m]	Autumn 14.09.	Bare	1 308	0.04	0.25	0.11	0.03	0.10	0.09
		Pond	887	0.05	0.32	0.14	0.05	0.13	0.10
Ice Thickness [m]	Autumn 14.09.	Bare	26 831	1.25	2.83	1.90	0.21	1.92	2.00
		Pond	18 794	1.14	2.32	1.73	0.19	1.75	1.80
Transmittance [%]	Summer 24.08.	Bare	830	0.7	15.5	4.1	1.9	3.9	4.5
		Pond	859	1.6	23.2	8.9	5.5	7.1	5.5
	Autumn 13.09.	Bare	466	0.2	3.4	1.8	0.7	1.9	2.0
		Pond	328	0.4	3.1	1.3	0.6	1.2	1.0

References

- Ehn, J. K., Papakyriakou, T. N., & Barber, D. G. (2008). Inference of optical properties from radiation profiles within melting landfast sea ice. *Journal of Geophysical Research*, 113(C09024). doi:10.1029/2007jc004656
- Katlein, C., Valcic, L., Lambert-Girard, S., & Hoppmann, M. (2021). New insights into radiative transfer within sea ice derived from autonomous optical propagation measurements. *The Cryosphere*, 15(1). doi:10.5194/tc-15-183-2021

- Light, B., Grenfell, T. C., & Perovich, D. K. (2008). Transmission and absorption of solar radiation by Arctic sea ice during the melt season. *Journal of Geophysical Research*, 113(C03023). doi:10.1029/2006jc003977
- Perovich, D. K. (1990). Theoretical estimates of light reflection and transmission by spatially complex and temporally varying sea ice covers. *Journal of Geophysical Research*, 95(C6). doi:10.1029/JC095iC06p09557
- Petrich, C., Nicolaus, M., & Gradinger, R. (2012b). Sensitivity of the light field under sea ice to spatially inhomogeneous optical properties and incident light assessed with three-dimensional Monte Carlo radiative transfer simulations. *Cold Regions Science and Technology*, 73. doi:10.1016/j.coldregions.2011.12.004